IJMMM International Journal of Minerals, Metallurgy and Materials 矿物冶金与材料学报（英文版）

Effects of highly dispersed Ni nanoparticles on the hydrogen storage performance of MgH_2

Nuo Xu, Zirui Yuan, Zhihong Ma, Xinli Guo, Yunfeng Zhu, Yongjin Zou, and Yao Zhang

Cite this article as:
Nuo Xu, Zirui Yuan, Zhihong Ma, Xinli Guo, Yunfeng Zhu, Yongjin Zou, and Yao Zhang, Effects of highly dispersed Ni nanoparticles on the hydrogen storage performance of MgH_2, *Int. J. Miner. Metall. Mater.*, 30(2023), No. 1, pp. 54-62. https://doi.org/10.1007/s12613-022-2510-8

International Journal of Minerals, Metallurgy and Materials
Volume 30, Number 1, January 2023, Page 54
https://doi.org/10.1007/s12613-022-2510-8

Effects of highly dispersed Ni nanoparticles on the hydrogen storage performance of MgH_2

Nuo Xu[1),*], *Zirui Yuan*[1),*], *Zhihong Ma*[2),*], *Xinli Guo*[1)], *Yunfeng Zhu*[3)], *Yongjin Zou*[4)], *and Yao Zhang*[1),✉]

1) School of Materials Science and Engineering, Jiangsu Key Laboratory of Advanced Metallic Materials, Southeast University, Nanjing 211189, China
2) School of Materials Science and Engineering, Baise University, Baise 533000, China
3) College of Materials Science and Engineering, Jiangsu Collaborative Innovation Centre for Advanced Inorganic Function Composites, Nanjing Tech University, Nanjing 211816, China
4) Guangxi Key Laboratory of Information Materials, Guilin University of Electronic Technology, Guilin 541004, China
(Received: 4 January 2022; revised: 25 April 2022; accepted: 28 April 2022)

Abstract: MgH_2 with a large hydrogen capacity is regarded as a promising hydrogen storage material. However, it still suffers from high thermal stability and sluggish kinetics. In this paper, highly dispersed nano-Ni has been successfully prepared by using the polyol reduction method with an average size of 2.14 nm, which significantly improves the de/rehydrogenation properties of MgH_2. The MgH_2–10wt% nano-Ni sample starts releasing H_2 at 497 K, and roughly 6.2wt% H_2 has been liberated at 583 K. The rehydrogenation kinetics of the sample are also greatly improved, and the adsorption capacity reaches 5.3wt% H_2 in 1000 s at 482 K and under 3 MPa hydrogen pressure. Moreover, the activation energies of de/rehydrogenation of the MgH_2–10wt% nano-Ni sample are reduced to (88 ± 2) and (87 ± 1) $kJ \cdot mol^{-1}$, respectively. In addition, the thermal stability of the MgH_2–10wt% nano-Ni system is reduced by 5.5 kJ per mol H_2 from that of pristine MgH_2. This finding indicates that nano-Ni significantly improves both the thermodynamic and kinetic performances of the de/rehydrogenation of MgH_2, serving as a bifunctional additive of both reagent and catalyst.

Keywords: Ni nanoparticle; kinetics; thermodynamics; MgH_2; hydrogen storage performance

1. Introduction

Currently, fossil fuels provide 80% of the global energy demand. Unfortunately, they also cause environmental pollution and greenhouse effects [1]. The need to find renewable and clean energy to replace fossil energy has become a global consensus [2]. Hydrogen has attracted extensive interest from all over the world as an efficient and sustainable secondary energy. The so-called hydrogen economy consists of the production, storage, and transportation of hydrogen, as well as hydrogen energy applications. However, hydrogen storage has always been a bottleneck that hampers the application of hydrogen [3–7].

During the past decade, many hydrogen storage materials and technologies have been developed [8]. MgH_2 has received much attention among these solid-state hydrogen storage materials because of its light weight, abundant reserves, non-toxic nature, and large hydrogen storage capacity, which has considerable potential for use in hydrogen fuel cells [9–12]. Excellent solid-state hydrogen storage materials should be capable of absorbing or releasing a large amount of hydrogen rapidly under low pressure and ambient temperature [13]. However, due to the high thermodynamic stability and retarded reaction kinetics of MgH_2, the system delivers a high operating temperature and sluggish hydrogen absorption/desorption rate, making it difficult to meet the requirements of practical applications [14–18]. Many efforts, such as alloying, nanosizing, and catalyst doping, have been made to overcome these issues [19–25]. Zhang *et al.* [26] successfully synthesized ultrafine MgH_2 nanoparticles of 4–5 nm, which can achieve a reversible hydrogen storage of 6.7wt% at room temperature. Adding catalysts could effectively lower the working temperature of hydrogen storage, enhance the desorption, and increase the reversible absorption rate of hydrogen [27–30]. Theoretically, the doped catalyst can provide favorable charge transfer and promote heat transfer in the MgH_2 system by generating many defects on the surface of MgH_2 [31–32].

In general, nanoscale catalysts can be in close contact with MgH_2 to create more active sites. Therefore, nanoscale catalysts can improve the hydrogen storage performance of MgH_2 [33]. Many studies have been conducted on transition metal catalysts in recent years [34–35]. Specifically, the transition metals Fe, Co, Ni, and Cu, for example, have been proven to play an important role in enhancing the hydrogen storage properties of MgH_2 [36]. The Ni-doped MgH_2 com-

* These authors contributed equally to this work.
✉ Corresponding author: Yao Zhang E-mail: zhangyao@seu.edu.cn

posite, in particular, exhibits exceptional catalytic performance [37]. Yu *et al.* [38] and Xie *et al.* [39] found that introducing the transition metals Fe, Co, Ni, Cu, and Zn into MgH_2 during the ball milling or dehydrogenation/absorption cycle processes will form numerous defects at the interfaces of Fe/MgH_2, Co/MgH_2, Ni/MgH_2, etc., respectively. Such defects considerably aid the splitting of H_2 molecules and the recombination of hydrogen atoms. Moreover, Chen *et al.* [40] investigated the hydrogen storage performance of the MgH_2–Ni/TiO_2 system and found that metallic Ni particles could easily react with Mg to yield Mg_2Ni compound during the dehydrogenation process, and the *in-situ* produced Mg_2Ni is converted into Mg_2NiH_4 during the subsequent rehydrogenation, acting as a hydrogen pump. Shao *et al.* [41] prepared a stable Ni-metal organic framework (MOFs) catalyst with uniform and dispersed Ni atoms that can improve the hydrogen storage performance of the MgH_2 system. Huang *et al.* [42] created highly dispersed metal-supported catalysts, including a series of 3d transition elements, La and Ce, on N-doped carbon (M–N–C). The kinetics of MgH_2–M–N–Cs were correlated with the electronegativity of M in M–N–Cs (V, Cr, Fe, Co, Ni, Cu, Zn), indicating that M–N–Cs with high electronegativity core elements can enhance the kinetics. In addition, MgH_2–Ni–N–C500 with the highest electronegativity (Ni, 1.91) was demonstrated remarkable kinetic performance. Zhang *et al.* [43] synthesized a series of nickel-based compounds (Ni_3C, Ni_3N, NiO, and Ni_2P) and found that the catalyst obtained by combining Ni with low electronegativity elements (Ni_3C) better enhanced the hydrogen storage performance of the MgH_2 system. In addition, El-Eskandarany *et al.* [44] employed Ni spheres as a grinding medium, progressively doping Ni spheres into MgH_2 powder. Their samples after ball milling exhibited a low dehydrogenation temperature (491 K) and a dehydrogenation activation energy (75 $kJ \cdot mol^{-1}$). Recent research has found that the size of the Ni particles has a major impact on the adsorption and dehydrogenation kinetics of MgH_2. Si *et al.* [45] discovered that the initial dehydrogenation temperature of the MgH_2–5wt% nano-Ni/C system was significantly reduced by 453 K, and the hydrogen absorption kinetics of the system was noticeably increased by 16-fold compared with that of the original MgH_2. Gao *et al.* [46] created Ni/Ti_3C_2 catalysts with interfacial differences and discovered that when Ni had the smallest particle size and best dispersibility at the Ti_3C_2 matrix interface, the most effective catalytic activity was produced. Chen *et al.* [47] synthesized Ni nanofibers with a uniform diameter of 50 nm and a porous structure composed of many Ni nano-crystallites, which were easily broken into superfine Ni nanoparticles with an average diameter of 17 nm by ball milling and uniformly dispersed on the surface of MgH_2. The hydrogen storage significantly improves the performance of MgH_2. Zhu *et al.* [48] designed a self-assembled two-dimensional MXene-based catalyst (2D-Ni@Ti_3C_2) whose Ni particles had an average size of less than 50 nm, and smaller particles were in the range of 5 nm. The MgH_2 + Ni@Ti–MX composite absorbed 5.4wt% H_2 in 25 s at 398 K and released 5.2wt% H_2 in 15 min at 523 K, demonstrating enhanced hydrogen storage performance. Therefore, the particle size of the catalyst and its close contact with MgH_2 determine its catalytic performance. Rahmalina *et al.* [49] also proved that reducing the size of Ni particles is the best approach to enhance the thermodynamic and kinetic performance of MgH_2. However, the best size of Ni and its size effect on the de/rehydrogenation performance still remain unclear.

In this paper, we focus on the effect and mechanism of nano-Ni particles on the thermal stability and catalytic performance of MgH_2. Ni particles with size of 1.5–2.5 nm have been successfully synthesized in this work. The effect of nano-Ni particle size on the MgH_2 system has been systematically studied, along with the catalytic mechanism of nano-Ni on the MgH_2 system.

2. Experimental

2.1. Preparation of the MgH_2–nano-Ni

The overall synthesis process of nano-Ni particles is shown in Fig. 1. First, 1.8 g sodium hydroxide (97%, Aladdin), 0.2241 g nickel acetate tetrahydrate (99%, Aladdin), 2.05 g oleic acid (analytical reagent (AR), Macklin), 0.5 g polyvinylpyrrolidone (PVP, guaranteed reagent (GR), Sinopharm), and 150 mL of 1,2-propylene glycol (AR, Sinopharm) were placed in a round-bottom flask. The temperature was increased to 389 K, and the reagents completely dis-

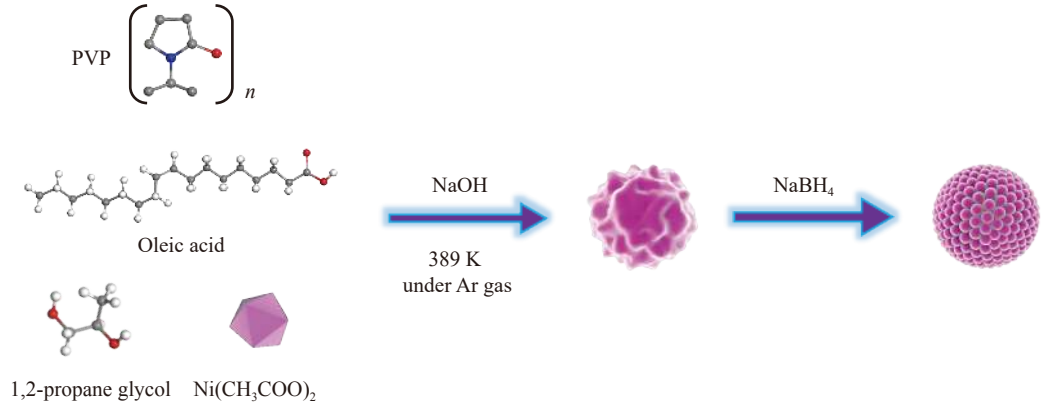

Fig. 1. Illustration of the synthesis of the nano-Ni composite.

solved with continuous magnetic stirring. The semi-products were obtained by dropping 30 mL of 1,2-propylene glycol solution containing 0.486 g of potassium borohydride (98%, Aladdin) into the solution in a glove box filled with high-purity argon. Finally, the Ni nanoparticles were collected by centrifugation and vacuum drying at 353 K for 10 h.

The purchased MgH_2 (95%, Alfa Aesar) was mixed (QM-1SP, Nanjing) with the prepared *x*wt% nano-Ni (x = 0, 3, 5, 10, 15) at 450 r/min with a 40:1 ball-to-powder ratio for 5 h. All samples were treated in a glovebox (Mikrouna Super 1220/750), and their H_2O and O_2 levels were below 0.0001‰.

2.2. Structural and morphology characterization

The phase structure of the composite system was determined by X-ray diffraction (XRD) and *in-situ* XRD (Rigaku) patterns. The morphology was characterized by transmission electron microscopy (TEM) and scanning electron microscopy (SEM), respectively. High-magnification images were obtained by using a high-resolution transmission electron microscope (HRTEM, FEI Tecnai G2 T20). The microstructure of the phases was analyzed by selected area electron diffraction (SAED).

2.3. De/rehydrogenation performances

The non-isothermal dehydrogenation performance was evaluated by using the volume release method (VR), from which the initial dehydrogenation temperature, the final dehydrogenation temperature, and the dehydrogenation capacity of the samples were identified. Dehydrogenation onset, peak, and cut-off temperatures were determined by temperature-programmed desorption (TPD) with online mass spectrometry (MS, Hiden, UK). The isothermal hydrogenation curves of the MgH_2–nano-Ni system were measured at 394, 421, 450, and 482 K, respectively, under 3 MPa. The pressure-composition isotherm curves (PCI) of MgH_2 and MgH_2–nano-Ni were tested at different temperatures. Differential scanning calorimetry (DSC) was performed on a TA Q2000 instrument, and approximately 5 mg of each sample was heated from room temperature to 773 K at 5, 10, 15, and 20 $K \cdot min^{-1}$, respectively.

3. Results and discussion

3.1. Characterization of nano-Ni

The TEM images in Fig. 2(a) and (b) show that the prepared catalyst powders are nanoclusters of extremely fine particles formed by agglomeration. The calculated average particle size is 2.14 nm, as indicated by the Nano Measure software, and the particle size is concentrated at 1.5–2.5 nm. This finding indicates that the particle size is relatively uniform, much smaller than that reported in many previous works [44–45,49–50], which should benefit the catalytic activity of the catalyst. The XRD pattern of the nanoparticles is displayed in Fig. 2(c), and all diffraction peaks correspond to Ni (111), Ni (200), and Ni (220), respectively. This finding demonstrates that the Ni precursor is completely reduced to metallic Ni after preparation. In addition, the diffraction peaks broaden while their intensities weaken, further indicating that the Ni nanoparticles are relatively small.

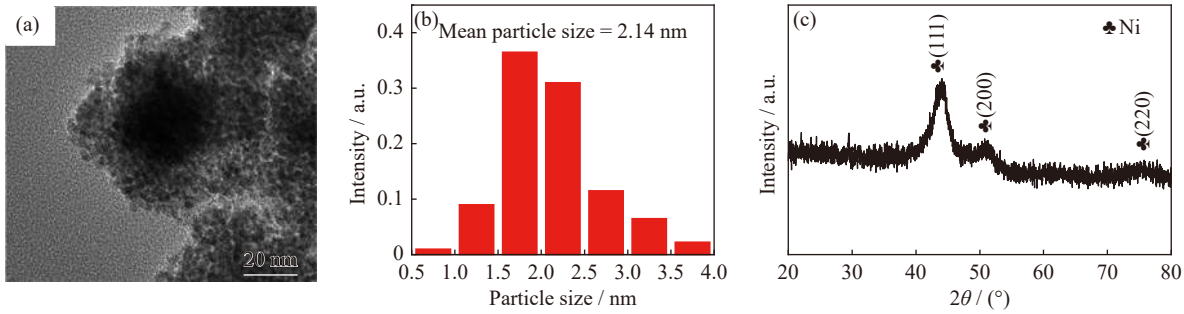

Fig. 2. (a) TEM image of the as-prepared nano-Ni. (b) Particle size distribution of the as-prepared nano-Ni. (c) XRD pattern of the as-prepared nano-Ni.

3.2. Effects of nano-Ni on the MgH_2 system

Fig. 3(a) displays the VR curves at a heating rate of 5 $K \cdot min^{-1}$ of MgH_2–*x*wt% nano-Ni (x = 0, 3, 5, 10, 15) samples. Its initial desorption temperature, final desorption temperature, and desorption capacity can be calculated as summarized in Table 1. Evidently, the system MgH_2–*x*wt% nano-Ni (x = 3, 5, 10, 15) starts to release hydrogen in the temperature range of 492–518 K, which is remarkably lower than the 580 K for the original MgH_2 sample. MgH_2–3wt% nano-Ni begins to release hydrogen at approximately 518 K, which is 62 K lower than that of undoped MgH_2. In addition, the dehydrogenation temperatures of MgH_2–5wt% nano-Ni, MgH_2–10wt% nano-Ni, and MgH_2–15wt% nano-Ni are further lowered to 510, 497, and 492 K, respectively. Furthermore, the three samples are dehydrogenated by the addition of nano-Ni before 672 K, with hydrogen releases of 6.5wt%, 6.2wt%, and 5.9wt%, respectively. The MgH_2–15wt% nano-Ni sample delivers an end temperature higher than the MgH_2–10wt% nano-Ni sample; thus, the MgH_2–10wt% nano-Ni sample seems to be the best choice for this work.

Fig. 3(b) shows the TPD-MS curves of the MgH_2 and MgH_2–10wt% nano-Ni samples at a heating rate of 5 $K \cdot min^{-1}$. For the sample doped by the nano-Ni catalyst, the dehydrogenation peak is apparently shifted to a lower temperature. The peak dehydrogenation temperature of the

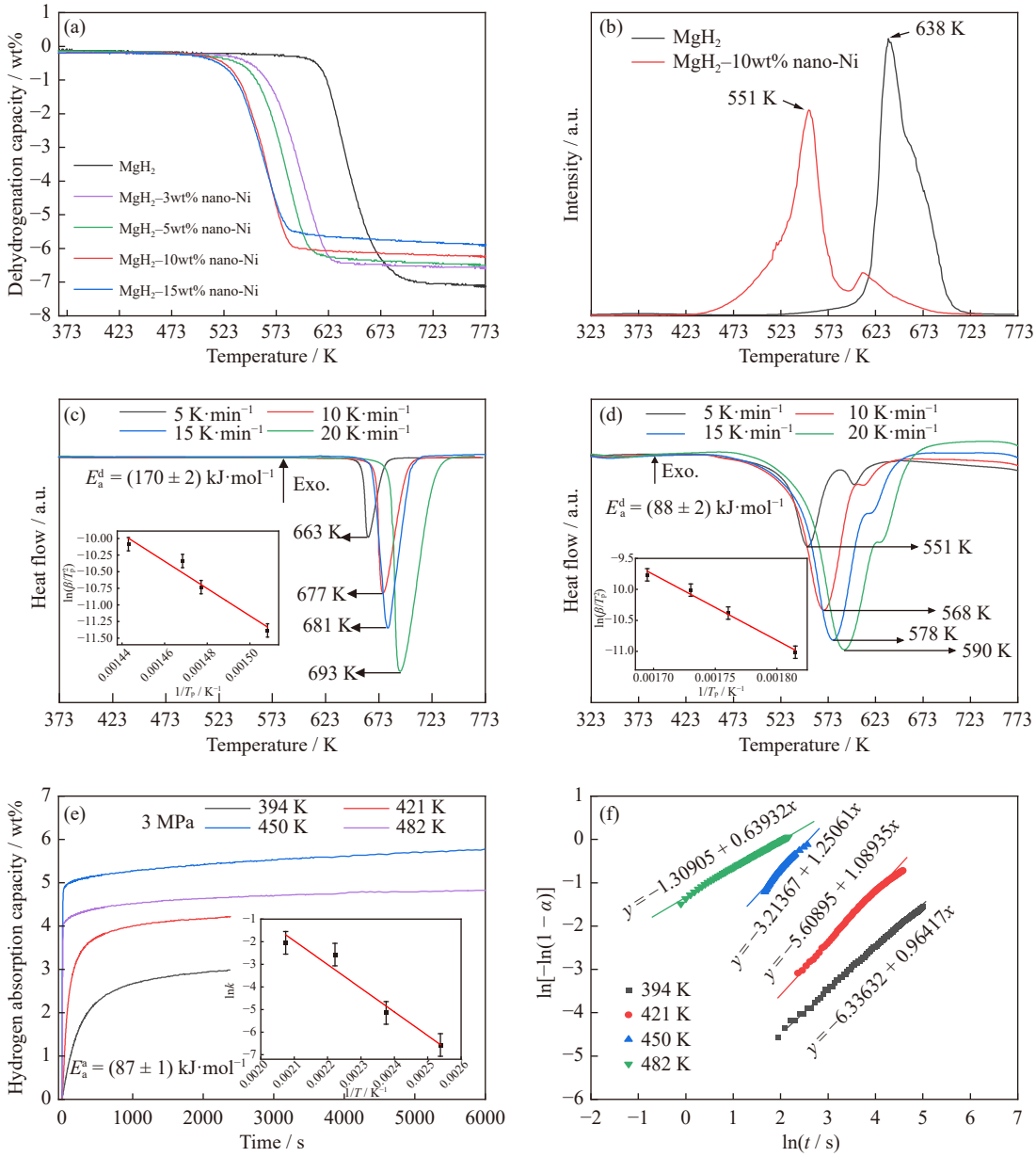

Fig. 3. (a) Volumetric release curves of as-milled MgH_2–*x*wt% nano-Ni (*x* = 0, 3, 5, 10, 15); (b) TPD-MS curves of the samples of MgH_2–10wt% nano-Ni and MgH_2. The temperature ramping rates are all 5 K·min^{-1}. DSC curves of the (c) as-milled MgH_2 and (d) MgH_2–10wt% nano-Ni, respectively; the insertion plots show the activation energies of the samples. (e) Isothermal hydrogenation curves of MgH_2–10wt% nano-Ni at different temperatures; inset is their Arrhenius plots. (f) The fitted lines reflecting the relationship of ln[−ln(1−α)]–ln$t$ built on the basis of the JMA equation; the slope stands for the activation energy E_a^a.

Table 1. Volumetric release curves of as-milled MgH_2–*x*wt% nano-Ni (*x* = 0, 3, 5, 10, 15)

Sample	Initial desorption temperature / K	End desorption temperature / K	Dehydrogenation capacity / wt%
MgH_2	580	672	7.2
MgH_2–3wt% nano-Ni	518	621	6.6
MgH_2–5wt% nano-Ni	510	605	6.5
MgH_2–10wt% nano-Ni	497	583	6.2
MgH_2–15wt% nano-Ni	492	585	5.9

MgH_2–10wt% nano-Ni sample is significantly reduced by 87 K compared with that of pure MgH_2. In addition, a minor dehydrogenation peak occurs at 673 K after ball milling of pure MgH_2, which is probably caused by the heterogeneous distribution of magnesium hydride particle size according to Ref. [51].

To further investigate the desorption kinetics, DSC measurements of MgH_2 and MgH_2–10wt% nano-Ni samples were

performed, as displayed in Fig. 3(c) and (d). The dehydrogenation temperature of MgH_2 is significantly lowered by nano-Ni. The endothermic peak of MgH_2–10wt% nano-Ni is 112 K lower than that of the original MgH_2. According to the different heating rates of DSC curves, the activation energy for desorption was calculated by Kissinger's equation [52], as shown in Eq. (1),

$$\frac{\mathrm{d}\left[\ln\left(\frac{\beta}{T_\mathrm{p}^2}\right)\right]}{\mathrm{d}\left(\frac{1}{T_\mathrm{p}}\right)} = -\frac{E_\mathrm{a}^\mathrm{d}}{R} \tag{1}$$

where β represents the heating rate, E_a^d denotes the activation energy for desorption, T_p stands for the endothermic peak temperature, and R is the gas constant. The activation energy of the MgH_2–10wt% nano-Ni system decreased to (88 ± 2) kJ·mol^{-1}, indicating that the nano-Ni additive could alleviate the kinetic barrier of MgH_2 dehydrogenation and greatly improve the MgH_2 dehydrogenation kinetics.

Aside from the remarkable improvement in the dehydrogenation properties, the hydrogen adsorption kinetics of the MgH_2–10wt% nano-Ni sample were also investigated. Isothermal hydrogen absorption measurements are shown in Fig. 3(e) and (f). An Arrhenius equation [53] could be established according to the following equation (Eq. (2)):

$$\ln k = -\frac{E_\mathrm{a}^\mathrm{a}}{RT} + \ln A \tag{2}$$

$$\alpha = 1 - \mathrm{e}^{-(kt)^n} \tag{3}$$

where k is the reaction rate constant, E_a^a denotes the activation energy of hydrogen absorption, T is the temperature, R stands for the gas constant, and A is the pre-exponential factor. In Eq. (3), α is the hydrogen absorption rate, which represents the ratio of the sample hydrogen absorption capacity to the saturation hydrogen absorption capacity at a certain time, n is Avrami index, and t is the reaction time. The activation energy (E_a^a) was calculated as (87 ± 1) kJ·mol^{-1} by using the Arrhenius formula and the John–Mehl–Avrami (JMA) formula (Eq. (3)) [54]. As shown in Fig. 3(e), as the hydrogen absorption temperature of MgH_2–10wt% nano-Ni increases, the saturated hydrogenation capacity gradually increases. In particular, the sample could rapidly absorb 5.3wt% H_2 within 1000 s at 482 K and under 3 MPa hydrogen pressure. In addition, the sample could absorb a total of 3wt% H_2 at 394 K. However, Fig. 4 shows that under the same conditions (482 K, 3 MPa H_2), reabsorbing hydrogen is difficult for MgH_2 after dehydrogenation, which indicates that the hydrogen absorption performance of MgH_2 can be significantly improved by the addition of nano-Ni.

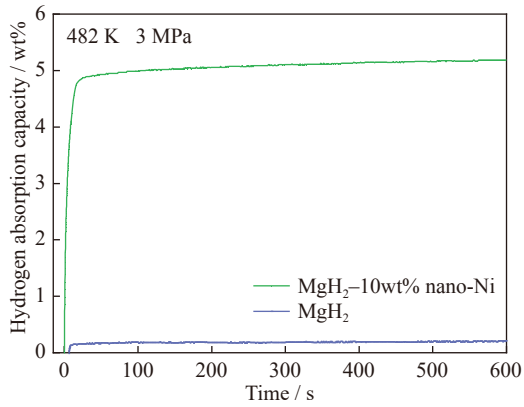

Fig. 4. Isothermal rehydrogenation curves of as-milled MgH_2 and MgH_2–10wt% nano-Ni composite at a temperature of 482 K under 3 MPa H_2.

The PCI curves of MgH_2 were measured at 647, 676, 681, and 698 K, and the MgH_2–10wt% nano-Ni sample was measured at 565, 587, 591, and 604 K, as shown in Fig. 5(a) and (b). Their Van 't-Hoff plots are shown in the insets of Fig. 5(a) and (b). The dehydrogenation enthalpy of MgH_2–10wt% nano-Ni and original MgH_2 were calculated by using the Van 't Hoff equation (Eq. (4)) [55].

$$\ln\left(\frac{P}{P_0}\right) = \frac{1}{T}\left(\frac{-\Delta H}{R}\right) + C \tag{4}$$

where P and P_0 represent the equilibrium atmosphere and the normal atmosphere (100 kPa), respectively; T is the temperature; ΔH means the enthalpy of desorption; R is the gas constant; C represents a constant whose value is equal to $\Delta S/R$, where ΔS is the entropy change (the value of the metal hydride is usually 130 J·mol^{-1}·K^{-1}. The dehydrogenation enthalpy value shifts slightly from (77.7 ± 0.5) kJ per mol H_2 for the original MgH_2 to (72.2 ± 0.5) kJ per mol H_2 for the

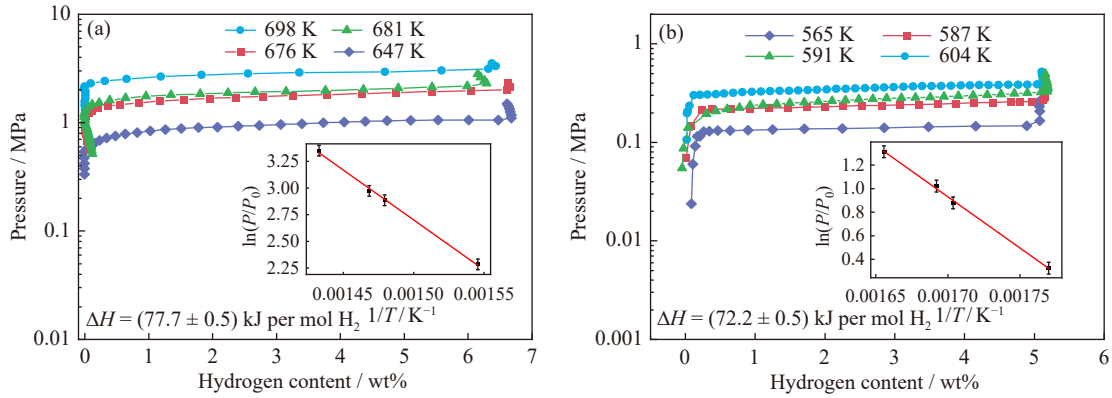

Fig. 5. PCI curves of (a) as-milled MgH_2 and (b) MgH_2–10wt% nano-Ni sample; the inserted Van 't Hoff plots show the dehydrogenation enthalpy values of the samples.

MgH_2–10wt% nano-Ni sample, as shown in Fig. 5(a). Hence, additional nano-Ni should be the main cause of the lower initial dehydrogenation temperature of the dehydrogenation. Therefore, we can conclude that nano-Ni might play a role in destabilizing MgH_2 during dehydrogenation.

3.3. Reaction mechanism

The diffraction peaks of the metallic Mg phase appear at 503 K, indicating that the MgH_2–10wt% nano-Ni sample begins to decompose and release hydrogen at this temperature, as shown in Fig. 6. The diffraction peaks of the Mg phase (PDF: 017-0902) gradually become noticeable with increasing temperature. Meanwhile, the MgH_2 phase (PDF: 002-6624) gradually weakens and finally disappears at 673 K, suggesting that the dehydrogenation is completed. Small traces of MgO and $Mg(OH)_2$ are also detected in the XRD patterns, which could be attributed to the sample's brief exposure to air while transferred from the glove box to the holder.

The SAED patterns from TEM image and inverse Fourier transform are shown in Fig. 7(a) and (b). The plane with a spacing of 0.225 nm can be considered as lattice fringes of the MgH_2 (110) planes (Fig. 7(c)). Crystal planes with spacing up to 0.205 and 0.178 nm correspond to the (111) and (200) planes of Ni, respectively. Such results confirm that no intermediate phase is formed during the ball milling and the ball milling products are Ni and MgH_2. On account of the high surface free energy of small particles, the sample after ball milling presents an aggregation distribution of small particles, as shown in Fig. 7(d). The TEM and Fourier transform images of the MgH_2–10wt% nano-Ni composite after dehydrogenation are shown in Fig. 7(e) and (f). They confirm the presence of Mg (101), Mg (103), Ni (220), and Mg_2Ni (114) planes in the dehydrogenated products, as shown by the *in-situ* XRD in Fig. 6. We can speculate that nano-Ni is involved in the MgH_2 dehydrogenation.

Furthermore, as shown in Fig. 7(g) and (h), the (002) plane of MgH_2, the (111) plane of Ni, and the (220) and (400) planes of Mg_2NiH_4 can be recognized in the SAED patterns of the rehydrogenated sample. The appearance of the Mg_2NiH_4 phase indicates that the product Mg_2Ni, as an intermediate phase in the absorption/desorption process, could promote the reversible absorption and desorption of the system. This result is consistent with the PCI measurement results, where the system is slightly destabilized during dehydrogenation. For MgH_2–Ni, the dehydrogenation is as follows:

$$3MgH_2 + Ni \rightarrow Mg + Mg_2Ni + 3H_2 \quad (5)$$

The rehydrogenation could be expressed as follows:

$$Mg + H_2 \rightarrow MgH_2 \quad (6)$$

$$Mg_2Ni + 2H_2 \rightarrow Mg_2NiH_4 \quad (7)$$

For this system, the dehydrogenation for the second time is described as follows:

$$MgH_2 + Mg_2NiH_4 \rightarrow Mg + Mg_2Ni + 3H_2 \quad (8)$$

In addition, the Ni phase is identified during the dehydrogenation and rehydrogenation processes, indicating that some nano-Ni still plays a catalytic role in the system.

Previous work by Chen *et al.* [50] indicated that the onset dehydrogenation temperature of MgH_2 doped with 20–30 nm Ni particles is 490 K, and the final temperature is about 643

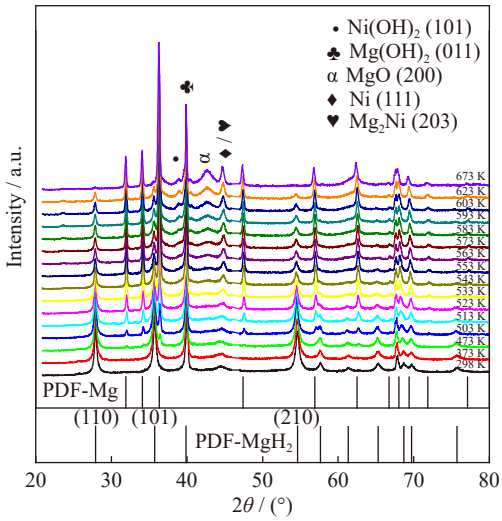

Fig. 6. ***In-situ*** **XRD patterns of MgH_2–10wt% nano-Ni from room temperature to 673 K.**

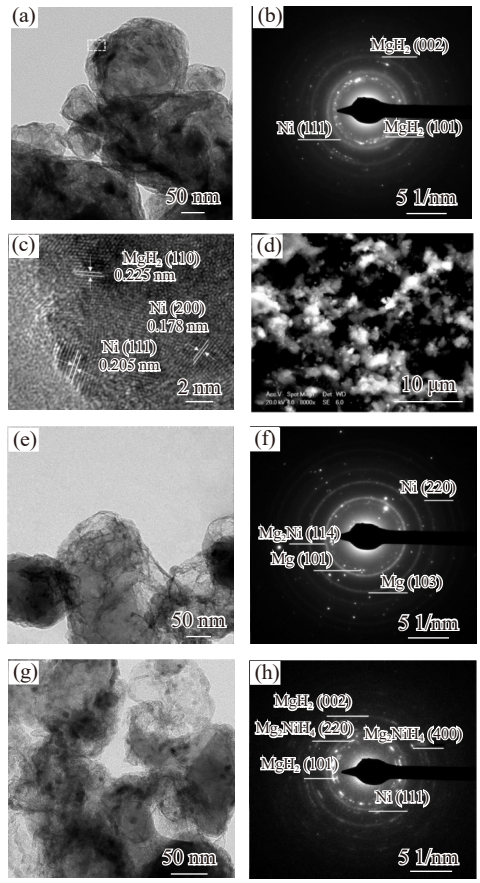

Fig. 7. (a) TEM, (b) SAED patterns, (c) HRTEM, and (d) SEM images of MgH_2–10wt% nano-Ni after preparation. (e) TEM image and (f) SAED patterns of the sample after dehydrogenation; those clusters are identified as Mg, Mg_2Ni, and Ni according to their SAED image. (g) TEM image and (h) SAED patterns of the sample after rehydrogenation remaining MgH_2, Mg_2NiH_4, and Ni phases.

K. As shown in Table 2, compared with their study, the final temperature in this work is decreased by 60 K, although the onset dehydrogenation temperature of MgH_2 catalyzed by nano-Ni with an average particle size of 2.14 nm is 497 K. This finding suggests that the Ni nanoparticles tend to agglomerate in the reaction and weaken the catalytic effect because of the loss of great active surfaces.

From the results obtained by Chen *et al.* [50], the dehydrogenation enthalpy of the MgH_2–Ni/CMK-3 system is decreased by 3 kJ per mol H_2, which is still 2.5 kJ per mol H_2 higher than that of the MgH_2–nano-Ni system. This result means that after ball milling, the small Ni nanoparticles should have a larger interface and be in closer contact with MgH_2, thus more actively participating in the reaction with MgH_2 and more effectively destabilizing the MgH_2 system than the large Ni nanoparticles can.

Table 2. Initial desorption temperature, end desorption temperature, and E_a^d of MgH_2–10wt% nano-Ni, MgH_2–10wt% Ni, and MgH_2

Sample	Initial desorption temperature / K	End desorption temperature / K	E_a^d / (kJ·mol^{-1})	ΔH / (kJ per mol H_2)
MgH_2 (This work)	580	672	170	77.7
MgH_2–10wt% nano-Ni (This work)	497	583	88	72.2
MgH_2–10wt% Ni [50]	490	643	121.8	—
MgH_2–10wt% Ni/CMK-3 [50]	433	568	43.4	74.7

4. Conclusion

Nano-Ni with an average particle size of 2.14 nm has been synthesized via the reduction method. The optimal MgH_2–10wt% nano-Ni starts to release hydrogen at 497 K and offers a dehydrogenation capacity of 6.2wt% below 583 K. The dehydrogenated MgH_2–10wt% nano-Ni system can absorb 5.3wt% H_2 in 1000 s at 482 K under 3 MPa hydrogen pressure. More remarkably, even at 394 K and 3 MPa hydrogen pressure, MgH_2–10wt% nano-Ni can uptake 3wt% hydrogen. In summary, the synthesized nano-Ni mainly exhibits excellent performance in reducing the enthalpy of dehydrogenation of MgH_2 and its decomposition. However, the catalytic activity is degraded as a result of the easy agglomeration of particles. Supporting materials such as CMK-3, reduced graphene oxide (rGO), and other carbon materials can be added to the support to disperse the catalysts and produce steady catalytic activity. Further work to avoid particle agglomeration is underway.

Acknowledgements

This work was financially supported by the National Natural Science Foundation of China (No. 52071177), the Natural Science Foundation of Guangxi, China (No. 2020GXNSFAA297074), the Jiangsu Key Laboratory for Advanced Metallic Materials (No. BM2007204), and the Guangxi Key Laboratory of Information Materials (No. 211021-K).

Conflict of Interest

The authors declare that they have no known competing financial interests or personal relationships that could have appeared to influence the work reported in this paper.

References

[1] X.L. Yang, J.Q. Zhang, Q.H. Hou, X.T. Guo, and G.Z. Xu, Improvement of Mg-based hydrogen storage materials by metal catalysts: Review and summary, *ChemistrySelect*, 6(2021), No. 33, p. 8809.

[2] T. He, H.J. Cao, and P. Chen, Complex hydrides for energy storage, conversion, and utilization, *Adv. Mater.*, 31(2019), No. 50, art. No. 1902757.

[3] Y.R. Wang, X.W. Chen, H.Y. Zhang, G.L. Xia, D.L. Sun, and X.B. Yu, Heterostructures built in metal hydrides for advanced hydrogen storage reversibility, *Adv. Mater.*, 32(2020), No. 31, art. No. 2002647.

[4] X. Zhao, S.M. Han, Y. Li, X.C. Chen, and D.D. Ke, Effect of $CeH_{2.29}$ on the microstructures and hydrogen properties of $LiBH_4$–Mg_2NiH_4 composites, *Int. J. Miner. Metall. Mater.*, 22(2015), No. 4, p. 423.

[5] Q. Li, X. Lin, Q. Luo, *et al.*, Kinetics of the hydrogen absorption and desorption processes of hydrogen storage alloys: A review, *Int. J. Miner. Metall. Mater.*, 29(2022), No. 1, p. 32.

[6] X.B. Yu, Z.W. Tang, D.L. Sun, L.Z. Ouyang, and M. Zhu, Recent advances and remaining challenges of nanostructured materials for hydrogen storage applications, *Prog. Mater. Sci.*, 88(2017), p. 1.

[7] M.D. Allendorf, Z. Hulvey, T. Gennett, *et al.*, An assessment of strategies for the development of solid-state adsorbents for vehicular hydrogen storage, *Energy Environ. Sci.*, 11(2018), No. 10, p. 2784.

[8] B. Sakintuna, F. Lamari-Darkrim, and M. Hirscher, Metal hydride materials for solid hydrogen storage: A review, *Int. J. Hydrogen Energy*, 32(2007), No. 9, p. 1121.

[9] I. Sreedhar, K.M. Kamani, B.M. Kamani, B.M. Reddy, and A. Venugopal, A Bird's Eye view on process and engineering aspects of hydrogen storage, *Renewable Sustainable Energy Rev.*, 91(2018), p. 838.

[10] J.Z. Song, Z.Y. Zhao, X. Zhao, R.D. Fu, and S.M. Han, Hydrogen storage properties of MgH_2 co-catalyzed by LaH_3 and NbH, *Int. J. Miner. Metall. Mater.*, 24(2017), No. 10, p. 1183.

[11] M. Hirscher, V.A. Yartys, M. Baricco, *et al.*, Materials for hydrogen-based energy storage –Past, recent progress and future outlook, *J. Alloys Compd.*, 827(2020), art. No. 153548.

[12] L.Z. Ouyang, X.S. Yang, M. Zhu, *et al.*, Enhanced hydrogen storage kinetics and stability by synergistic effects of *in situ* formed $CeH_{2.73}$ and Ni in $CeH_{2.73}$–MgH_2–Ni nanocomposites, *J. Phys. Chem. C*, 118(2014), No. 15, p. 7808.

[13] J.O. Abe, A.P.I. Popoola, E. Ajenifuja, and O.M. Popoola, Hydrogen energy, economy and storage: Review and recommendation, *Int. J. Hydrogen Energy*, 44(2019), No. 29, p. 15072.

[14] I.P. Jain, C. Lal, and A. Jain, Hydrogen storage in Mg: A most

promising material, *Int. J. Hydrogen Energy*, 35(2010), No. 10, p. 5133.
[15] J.F. Zhang, Z.N. Li, Y.F. Wu, *et al*., Recent advances on the thermal destabilization of Mg-based hydrogen storage materials, *RSC Adv.*, 9(2019), No. 1, p. 408.
[16] F. Dawood, M. Anda, and G.M. Shafiullah, Hydrogen production for energy: An overview, *Int. J. Hydrogen Energy*, 45(2020), No. 7, p. 3847.
[17] Q. Luo, J.D. Li, B. Li, B. Liu, H.Y. Shao, and Q. Li, Kinetics in Mg-based hydrogen storage materials: Enhancement and mechanism, *J. Magnes. Alloys*, 7(2019), No. 1, p. 58.
[18] X.B. Xie, C.X. Hou, C.G. Chen, *et al*., First-principles studies in Mg-based hydrogen storage materials: A review, *Energy*, 211(2020), art. No. 118959.
[19] C.S. Zhou, Z.Z. Fang, and P. Sun, An experimental survey of additives for improving dehydrogenation properties of magnesium hydride, *J. Power Sources*, 278(2015), p. 38.
[20] Z. Abdin, A. Zafaranloo, A. Rafiee, W. Mérida, W. Lipiński, and K.R. Khalilpour, Hydrogen as an energy vector, *Renewable Sustainable Energy Rev.*, 120(2020), art. No. 109620.
[21] L.Z. Ouyang, K. Chen, J. Jiang, X.S. Yang, and M. Zhu, Hydrogen storage in light-metal based systems: A review, *J. Alloys Compd.*, 829(2020), art. No. 154597.
[22] F. Li, X. Jiang, J.J. Zhao, and S.B. Zhang, Graphene oxide: A promising nanomaterial for energy and environmental applications, *Nano Energy*, 16(2015), p. 488.
[23] P. Rizo-Acosta, F. Cuevas, and M. Latroche, Hydrides of early transition metals as catalysts and grain growth inhibitors for enhanced reversible hydrogen storage in nanostructured magnesium, *J. Mater. Chem. A*, 7(2019), No. 40, p. 23064.
[24] L.Z. Ouyang, F. Liu, H. Wang, *et al*., Magnesium-based hydrogen storage compounds: A review, *J. Alloys Compd.*, 832(2020), art. No. 154865.
[25] E. Boateng and A.C. Chen, Recent advances in nanomaterial-based solid-state hydrogen storage, *Mater. Today Adv.*, 6(2020), art. No. 100022.
[26] X. Zhang, Y.F. Liu, Z.H. Ren, *et al*., Realizing 6.7 wt.% reversible storage of hydrogen at ambient temperature with non-confined ultrafine magnesium hydrides, *Energy Environ. Sci.*, 14(2021), No. 4, p. 2302.
[27] J.C. Crivello, B. Dam, R.V. Denys, *et al*., Review of magnesium hydride-based materials: Development and optimisation, *Appl. Phys. A*, 122(2016), No. 2, art. No. 97.
[28] H. Wang, H.J. Lin, W.T. Cai, L.Z. Ouyang, and M. Zhu, Tuning kinetics and thermodynamics of hydrogen storage in light metal element based systems – A review of recent progress, *J. Alloys Compd.*, 658(2016), p. 280.
[29] H.Y. Shao, L.Q. He, H.J. Lin, and H.W. Li, Progress and trends in magnesium-based materials for energy-storage research: A review, *Energy Technol.*, 6(2018), No. 3, p. 445.
[30] Y. Wang and Y.J. Wang, Recent advances in additive-enhanced magnesium hydride for hydrogen storage, *Prog. Nat. Sci. Mater. Int.*, 27(2017), No. 1, p. 41.
[31] M.E. Khatabi, M. Bhihi, S. Naji, *et al*., Study of doping effects with 3d and 4d-transition metals on the hydrogen storage properties of MgH_2, *Int. J. Hydrogen Energy*, 41(2016), No. 8, p. 4712.
[32] S. Chakrabarti and K. Biswas, Effect on de-hydrogenation efficiency on doping of rare earth elements (Pr, Nd, Gd, Dy) in MgH_2 – A density functional theory study, *Int. J. Hydrogen Energy*, 42(2017), No. 2, p. 1012.
[33] X.L. Zhang, Y.F. Liu, X. Zhang, J.J. Hu, M.X. Gao, and H.G. Pan, Empowering hydrogen storage performance of MgH_2 by nanoengineering and nanocatalysis, *Mater. Today Nano*, 9(2020), art. No. 100064.
[34] V.A. Yartys, M.V. Lototskyy, E. Akiba, *et al*., Magnesium based materials for hydrogen based energy storage: Past, present and future, *Int. J. Hydrogen Energy*, 44(2019), No. 15, p. 7809.
[35] Z. Sun, X. Lu, F.M. Nyahuma, *et al*., Enhancing hydrogen storage properties of MgH_2 by transition metals and carbon materials: A brief review, *Front. Chem.*, 8(2020), art. No. 552.
[36] N. Hanada, T. Ichikawa, and H. Fujii, Catalytic effect of nanoparticle 3d-transition metals on hydrogen storage properties in magnesium hydride MgH_2 prepared by mechanical milling, *J. Phys. Chem. B*, 109(2005), No. 15, p. 7188.
[37] M. Lakhal, M. Bhihi, A. Benyoussef, A.E. Kenz, M. Loulidi, and S. Naji, The hydrogen ab/desorption kinetic properties of doped magnesium hydride MgH_2 systems by first principles calculations and kinetic Monte Carlo simulations, *Int. J. Hydrogen Energy*, 40(2015), No. 18, p. 6137.
[38] H. Yu, S. Bennici, and A. Auroux, Hydrogen storage and release: Kinetic and thermodynamic studies of MgH_2 activated by transition metal nanoparticles, *Int. J. Hydrogen Energy*, 39(2014), No. 22, p. 11633.
[39] L.S. Xie, J.S. Li, T.B. Zhang, and H.C. Kou, Understanding the dehydrogenation process of MgH_2 from the recombination of hydrogen atoms, *Int. J. Hydrogen Energy*, 41(2016), No. 13, p. 5716.
[40] M. Chen, X.Z. Xiao, M. Zhang, *et al*., Excellent synergistic catalytic mechanism of *in-situ* formed nanosized Mg_2Ni and multiple valence titanium for improved hydrogen desorption properties of magnesium hydride, *Int. J. Hydrogen Energy*, 44(2019), No. 3, p. 1750.
[41] H.X. Shao, Y.K. Huang, H.N. Guo, Y.F. Liu, Y.S. Guo, and Y.J. Wang, Thermally stable Ni MOF catalyzed MgH_2 for hydrogen storage, *Int. J. Hydrogen Energy*, 46(2021), No. 76, p. 37977.
[42] Y.K. Huang, C.H. An, Q.Y. Zhang, *et al*., Cost-effective mechanochemical synthesis of highly dispersed supported transition metal catalysts for hydrogen storage, *Nano Energy*, 80(2021), art. No. 105535.
[43] Q.Y. Zhang, L. Zang, Y.K. Huang, *et al*., Improved hydrogen storage properties of MgH_2 with Ni-based compounds, *Int. J. Hydrogen Energy*, 42(2017), No. 38, p. 24247.
[44] M.S. El-Eskandarany, E. Shaban, N. Ali, F. Aldakheel, and A. Alkandary, *In-situ* catalyzation approach for enhancing the hydrogenation/dehydrogenation kinetics of MgH_2 powders with Ni particles, *Sci. Rep.*, 6(2016), art. No. 37335.
[45] T.Z. Si, X.Y. Zhang, J.J. Feng, X.L. Ding, and Y.T. Li, Enhancing hydrogen sorption in MgH_2 by controlling particle size and contact of Ni catalysts, *Rare Met.*, 40(2021), No. 4, p. 995.
[46] H.G. Gao, R. Shi, J.L. Zhu, *et al*., Interface effect in sandwich like Ni/Ti_3C_2 catalysts on hydrogen storage performance of MgH_2, *Appl. Surf. Sci.*, 564(2021), art. No. 150302.
[47] J. Chen, G.L. Xia, Z.P. Guo, Z.G. Huang, H.K. Liu, and X.B. Yu, Porous Ni nanofibers with enhanced catalytic effect on the hydrogen storage performance of MgH_2, *J. Mater. Chem. A*, 3(2015), No. 31, p. 15843.
[48] W. Zhu, S. Panda, C. Lu, *et al*., Using a self-assembled two-dimensional MXene-based catalyst (2D-Ni@Ti_3C_2) to enhance hydrogen storage properties of MgH_2, *ACS Appl. Mater. Interfaces*, 12(2020), No. 45, p. 50333.
[49] D. Rahmalina, R.A. Rahman, A. Suwandi, and Ismail, The recent development on MgH_2 system by 16 wt.% nickel addition and particle size reduction through ball milling: A noticeable hydrogen capacity up to 5 wt.% at low temperature and pressure, *Int. J. Hydrogen Energy*, 45(2020), No. 53, p. 29046.
[50] G. Chen, Y. Zhang, J. Chen, X.L. Guo, Y.F. Zhu, and L.Q. Li, Enhancing hydrogen storage performances of MgH_2 by Ni nano-particles over mesoporous carbon CMK-3, *Nanotechnology*, 29(2018), No. 26, art. No. 265705.
[51] H.H. Cheng, G. Chen, Y. Zhang, Y.F. Zhu, and L.Q. Li, Boosting low-temperature de/re-hydrogenation performances of

MgH_2 with Pd–Ni bimetallic nanoparticles supported by mesoporous carbon, *Int. J. Hydrogen Energy*, 44(2019), No. 21, p. 10777.

[52] P. Plerdsranoy, S. Thiangviriya, P. Dansirima, *et al*., Synergistic effects of transition metal halides and activated carbon nanofibers on kinetics and reversibility of MgH_2, *J. Phys. Chem. Solids*, 124(2019), p. 81.

[53] T.P. Huang, J.X. Zou, H.B. Liu, and W.J. Ding, Effect of different transition metal fluorides TMF_x (TM=Nb, Co, Ti) on hydrogen storage properties of the $3NaBH_4$–GdF_3 system, *J. Alloys Compd.*, 823(2020), art. No. 153716.

[54] F.H. Wang, Y.F. Liu, M.X. Gao, K. Luo, H.G. Pan, and Q.D. Wang, Formation reactions and the thermodynamics and kinetics of dehydrogenation reaction of mixed alanate Na_2LiAlH_6, *J. Phys. Chem. C*, 113(2009), No. 18, p. 7978.

[55] N. Patelli, M. Calizzi, A. Migliori, V. Morandi, and L. Pasquini, Hydrogen desorption below 150°C in MgH_2–TiH_2 composite nanoparticles: Equilibrium and kinetic properties, *J. Phys. Chem. C*, 121(2017), No. 21, p. 11166.